Energy Conversion and Management 68 (2013) 114–123

Contents lists available at SciVerse ScienceDirect

Energy Conversion and Management

journal homepage: www.elsevier.com/locate/enconman

# Performance factors for ground-air thermoelectric power generators

James W. Stevens *

*Department of Mechanical and Aerospace Engineering, University of Colorado at Colorado Springs, Colorado Springs, CO 80920, United States*

ARTICLE INFO

*Article history:*
Received 30 April 2009
Received in revised form 4 December 2012
Accepted 30 December 2012
Available online 10 February 2013

*Keywords:*
Heat engines
Ground-source
Thermoelectrics
Energy harvesting
Temperature difference

ABSTRACT

The daily variation in air temperature is large compared with the temperature changes a short distance below the surface of the ground. In theory, a heat engine can be arranged to produce electricity from this temperature difference. In practice, the thermal efficiency of such a device will be low because of the small temperature differences involved. One example of such an energy harvesting device that can produce a small amount of electrical power uses a thermoelectric generator operating between the air and ground temperatures. The low thermal efficiency means that accurately predicting thermal resistances throughout the device and at the air-side and ground-side heat exchangers is critical to the creation of a useful device. Advantages of this device include high reliability, no acoustic emissions, low visibility, significant night-time power production, ruggedness, and long life. With appropriate external power conditioning components, the device could be used to power remote sensors and communications systems. The design of a pair of milliwatt-scale ground source heat engines is described. The devices were fabricated using custom heat exchangers and off-the-shelf thermoelectric modules and other supplies. Both systems were tested over an extended period in order to quantitatively assess effects of sunlight and precipitation on system performance and life. Exhaustive analysis of air-side average heat transfer coefficients, system thermal resistances, and ground-side thermal resistances provides quantitative design information for future applications. Finned and unfinned versions of otherwise identical prototypes permits assessment of fin performance on both ground-side and air-side heat transfer.



## 1. Introduction

Daily fluctuations in air temperature occur throughout most of the year and in most locations around the earth. The combined effects of a difference in heat capacity and conduction rates cause the ground temperature, even a short distance below the surface, to have lagging and damped temperature fluctuations. (Stevens [1]) In theory, this temperature difference can be used to power a heat engine to generate a small amount of electric power. In practice, the second law of thermodynamics dictates that the relatively small temperature difference will result in a low thermal efficiency; that is, large amounts of heat will have to be moved to generate even a modest amount of electricity. Therefore, the heat transfer characteristics of the air-side and ground-side heat exchangers becomes a dominant factor in the design and operation of a functional device.

This work describes the design and testing of two heat engines which generate electric power from the temperature difference between the air and the ground using thermoelectric modules. The objective of the work was to quantify thermal resistances and environmental effects in functional, practical devices operating in actual field conditions.

## 2. Literature review

Other ideas for energy harvesting using thermoelectric modules for the heat engine have been proposed.

Lemley [2] discussed an unusual application of a thermoelectric generator designed to produce power from the long wave infrared radiation from the surface of the earth. The proposed application was for a high altitude, long duration communications platform. Radiant energy would be collected from the earth, and heat would be rejected by radiation into space. A thin-film configuration was devised and limited tests were conducted. A temperature difference of 58 °C was used in the design. Weight would be a dominant factor in such an application while it is inconsequential in the current study, however, issues concerning practical thermal resistances and temperature drops which would be necessary to realize such a design are explored in this work.

Wu [3] analyzed the thermodynamics of a generator that would operate from industrial waste heat using thermoelectric modules. The same author performed a very similar analysis (Wu [4]) for a thermoelectric generator operating from a solar pond. The thermodynamic efficiency and specific work output were emphasized in both cases and comparisons were made with theoretical efficiencies.

Benson and Jayadev [5] explored the possibility of using thermoelectric generators to produce useful amounts of electricity

* Tel.: +1 719 255 3581.
*E-mail address:* JStevens@UCCS.edu

0196-8904/$ - see front matter © 2013 Elsevier Ltd. All rights reserved.
http://dx.doi.org/10.1016/j.enconman.2012.12.029

from low grade heat sources in large installations. One possibility discussed was to use thermoelectric generators in an Ocean Thermal Energy Conversion system. The proposed temperature difference for that case was 5–25 °C. It was shown that some commercially available thermoelectric materials have a very good figure of merit in this temperature range. An assumed performance of 20% of Carnot efficiency achieved by the thermoelectric devices was used for calculations. Other potential sources of energy that were discussed included geothermally heated ocean water (85 °C), solar ponds (50 °C), natural lake thermoclines (10–20 °C), and utility power plant waste heat (15 °C). Long term capital costs were considered in the discussion. At these temperature ranges, an understanding of achievable thermal resistances as treated in the current study, will be essential.

Chen [6] performed a thermodynamic analysis of a thermoelectric generator powered by direct solar radiation. The main conclusions of the analysis involved the establishment of performance limits for solar powered thermoelectric devices. In the current study, solar insolation has a significant but not dominant effect on the overall device operation.

Henderson [7] developed an analytical model for a small $\Delta T$ thermoelectric generator that includes the hot and cold side heat exchangers. The system power was optimized using Lagrange multipliers on a system of four non-linear equations. The solution was achieved via an iterative approach, but no closed form solution was determined. Analyses of several complete systems led to the empirical conclusion that the total temperature difference should be split equally between the thermoelectric module and the external heat exchangers. This result, also shown in [16], was used in configuring the prototype of this study.

Hudak and Amatucci [8] reviewed state-of-the-art energy harvesting focused on devices of cubic centimeter scale. In addition to harvesting concepts involving vibrational and radio frequency energy, they reviewed thermoelectric power generation from ambient heat sources, including a thorough review of thermoelectric power generation and fabrication of small devices. They emphasized the point that for energy harvesting from ambient sources, the temperatures and heat flow are not controlled, and that most literature tends to report $\Delta T$ across the generating device rather than the source heat flow, though the latter would be of more practical use in evaluating potential performance. In the current study, the description of thermal resistances takes into account both temperature differences and heat flows. They also considered power conditioning systems and problems with integrating small, low temperature thermoelectric power generators into useful generation systems including low voltages and intermittent power production. The electronics for power conditioning and/or power storage would have to be made small and cheaply to merit inclusion in low temperature generation devices.

Thomas et al. [9] examined thermoelectric energy scavenging with specific application to potentially extending flight time of small air vehicles. For moderate temperatures and commercially available materials, critical implementation issues for this application are centered around optimizing thermal performance and minimizing weight of the heat exchangers and support hardware. While weight is not typically a key factor in ground-based applications, all other aspects including designing for maximum thermal performance of the heat exchangers and optimizing matching with thermoelectric modules are similar.

Dalola et al. [10] tested three different commercially available thermoelectric modules designed for cooling/heating applications in low temperature difference power generation conditions, specifically aimed for applications involving powering autonomous sensors. Their measured results compared favorably to published specifications for three other commercially available modules designed specifically for power generation. They demonstrated an application where a thermoelectric module powering a system with a passive sensor and a radio frequency transmission link would function with a temperature difference as low as 34 K. Such an application would be similar to the kinds of uses for systems based on the prototypes of this study.

Sodano et al. [11] demonstrated battery charging for unattended structural health monitoring applications using thermoelectric generators connected directly to the batteries. The heat source for the thermoelectric generators consisted of a solar concentrator combined with a greenhouse-type enclosure to raise the temperatures sufficiently. They showed that such a system would be viable and could outperform piezoelectric energy harvesting by an order of magnitude in some applications.

Lawrence and Snyder [12] tested thermal conductance of ground-side heat exchangers for applications of thermoelectric generators harvesting energy from the temperature difference between the air and the ground. Heaters were used to impose a heat flow through the heat exchangers and thermal conductances were determined for several geometries. While the specific geometries were quite different from the ground-side heat exchanger of the present work, they determined that simple shape factors could be used to provide a rough estimate of the thermal performance of ground-side heat exchangers.

Meydbray et al. [13] experimentally examined the effect of surface area on air–ground thermoelectric generation by testing a thermoelectric module sandwiched between a large copper plate set in soil and various sized air-side aluminum-nitride plates. Open circuit voltages from the thermoelectric generator were measured. It was found that power generation increased significantly with increased surface area of the air-side plates. This result supports the findings of the current study with respect to controlling thermal resistances in the air-side heat exchangers.

Snyder [14] provided a comprehensive review of design of thermoelectric generation systems for energy harvesting including background and design considerations specific to energy harvesting applications.

Agbossou et al. [15] developed a detailed ANSYS model of a system which would couple a thermoelectric generator with a phase change material in order to harvest ambient energy from daily fluctuations in solar insolation. The model incorporated both heat transfer and thermoelectric generation phenomena to provide a detailed simulation based on assumed solar heating, atmospheric temperatures, and convective heat transfer off the exposed face of the thermoelectric module. The idea of the combined system is very similar to the idea underlying the work reported here, with the latent heat capacity of the phase change material taking the place of the effectively infinite thermal capacitance of the earth. They found that the total energy generation depends strongly on the intensity of the incident solar radiation, and that a smaller amount of energy harvesting can be achieved at night.

This paper reports on design and test results for a pair of prototype ground-source heat engines that produce small amounts of power from the daily temperature difference between the air and the ground. The prototypes were intended to provide a proof-of-concept demonstration as well as to provide quantitative data on device design and function that will be useful for practical design considerations in future applications.

## 3. Design description

The two prototype ground-source heat engines were built using off-the-shelf thermoelectric modules sandwiched between two heat exchangers. (Fig. 1) It has been shown (Stevens [16]) that for a given total temperature difference, the optimum distribution of temperature drop should be divided evenly between the

thermoelectric modules and all other thermal resistances. Unfortunately, the total thermal resistance of the heat exchangers is difficult to estimate accurately. It includes convection between the air and the air side heat exchanger surfaces, various conduction and contact resistances, and conduction through the ground. Convective heat transfer coefficients depend on the air temperature and wind speed. The convection coefficient could vary by an order of magnitude or more through the course of a single day. Conduction through the ground depends heavily on the soil type and moisture content of the soil. Shallow soil moisture levels exhibit significant variations with precipitation and relative humidity. Part of the objective of these prototype tests was to approximately quantify some of these thermal resistances.

The prototypes were constructed with HZ 2 thermoelectric modules from Hi-Z Technology, Inc. in San Diego, CA, USA. In order to approximate the optimum temperature drop configuration, (that is, the equal division of the total temperature drop between the drop across the thermoelectric modules and the drop due to all other thermal resistances) two modules were arranged thermally in series, as shown in Fig. 1, based on the design calculations. The modules were separated electrically from each other and from the metal heat exchangers by thin ceramic insulators. The sole purpose of these insulators was to prevent electrical short-circuit of the exposed module elements. In practice, these insulators were so thin that the thermal resistance through the ceramic insulators was negligible. The two prototypes had the same baseline dimensions and differed by the addition of fins on both the air-side and ground-side heat exchangers on one of the prototypes. (Fig. 2)

Thermal resistances between the air and the ground were identified as follows:

(1) Convection from the air to the air-side heat exchanger.
(2) Conduction through the air-side heat exchanger.
(3) Contact resistances and conduction through the first ceramic insulator.
(4) Conduction through the top thermoelectric module.
(5) Contact resistances and conduction through the second ceramic insulator.
(6) Conduction through the bottom thermoelectric module.

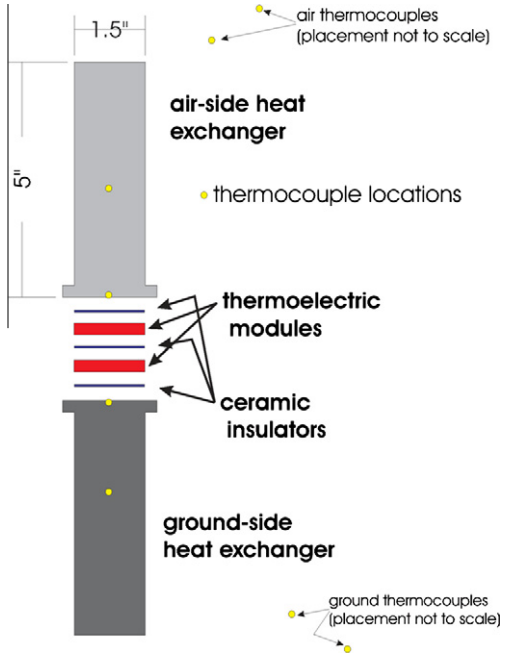


**Fig. 1.** Prototype layout.

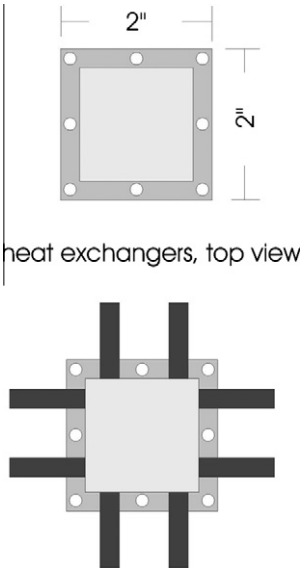


**Fig. 2.** Unfinned and finned configurations.

(7) Contact resistances and conduction through the third ceramic insulator.
(8) Conduction through the ground-side heat exchanger.
(9) Contact resistance between the ground-side heat exchanger and the soil.
(10) Conduction into the soil.

Using standard heat transfer calculations, it was estimated that all thermal resistances would be small relative to those due to convection with the air (1), conduction through the thermoelectric modules (4 and 6) and conduction through the soil (10). From manufacturer's data the thermal resistance through each thermoelectric module was estimated at 2.5 K/W. The sum of the air convection and ground-side conduction resistances was estimated to be 11 K/W for the unfinned prototype version. As mentioned previously, two thermoelectric modules were placed in series. While four modules in series would have been closer to the optimum, there are diminishing returns as the optimum is approached. For example, calculations indicated that while two modules would improve performance by 42% over a single module, three modules would only yield another 12% improvement and four modules an additional 4% improvement over three. Thus, the choice of two modules as the configuration for the prototypes represents a trade-off between performance and size/expense of the system.

The heat exchanger bodies were machined from solid aluminum and for the finned heat exchangers, the fins were aluminum welded to the heat exchanger body. The thermoelectric modules were secured between the heat exchangers with nylon screws in order to reduce an alternate heat conduction path that would bypass the thermoelectric modules. Thermal grease was used to minimize contact resistance between the ceramic insulators and all other surfaces. The thermoelectric modules were wired in series electrically, and the power output was discharged through a fixed resistor matched to the operating characteristics of the thermoelectric module.

## 4. Test description

Both prototypes were deployed at an outdoor test location in Colorado Springs, CO (38°56′N, 104°47′W) for a period of 25 days in May and June. Temperatures were recorded for the ambient air, several undisturbed underground locations to a depth of

approximately 14 in., the top and bottom heat exchangers for both prototypes, and the top and bottom insulator surfaces for both prototypes. Thermocouple placement locations are indicated in Fig. 1. In all cases thermocouples were 24 gauge, type *T* thermocouples manufactured by Omega. Thermocouples were installed in the center of each heat exchanger through a 3.2 mm blind hole drilled from the side. In each case, the hole was filled with thermally conductive paste, the thermocouple was inserted to the bottom of the hole, and tape was used to seal the hole and secure the protruding thermocouple wire. Installation of the thermocouples at the interfaces between the heat exchangers and ceramic insulating plates was accomplished in an identical manner, except the access hole was drilled at an angle in order to position the thermocouple at the interface. The air temperature thermocouples were shielded from direct sunlight, but otherwise left exposed to the open atmosphere. Some ground-side thermocouples were buried directly in the soil, and others were cemented with thermally conductive epoxy to the inside of a copper pipe which was then driven vertically into the ground. Both methods gave substantially identical results for similar depths.

Thermocouples and thermoelectric module output were recorded at 74 s intervals over the entire test period using an Omega A/D converter controlled by Labview software. For each recorded measurement, approximately 1400 individual samples were averaged by the data acquisition software. This resulted in an estimated maximum random error of 0.12 °C and an RMS random error of 0.03 °C for all temperature measurements. Absolute bias errors in temperature were estimated at 0.8 °C based on testing and manufacturer's literature. For the voltage measurements used to calculate the thermoelectric power generation, the maximum random error was 0.55 mV and the RMS random error was 0.23 mV. Absolute bias error in voltage was 0.01 mV. These uncertainties propagated through the calculations to give average uncertainties of 83 μW in reported power and 6 mJ in reported energy. The test period included days of sunshine and clouds as well as a few days with precipitation.

## 5. Test results

Figs. 3a and 3b shows the measured ambient air temperature as well as the undisturbed temperature of the ground (away from the prototype installations, and a few inches deeper than the ground side heat exchangers). For visibility, 2, 4-day periods were selected for display out of the total 25 day measurement span. (Figs. 3a and 3b) Over the period covered by Fig. 3a, the weather had intermittent overcast, with the heavy dashed line indicating periods of precipitation. During the time shown in Fig. 3b, the weather was predominantly clear. As a starting point, the difference between the air and ground temperatures could be considered to represent the maximum possible temperature difference for power generation from these devices. However, that maximum must be modified by two considerations. First, as indicated previously, the optimal design for power generation is to split the total available temperature difference between the thermoelectric modules and the heat exchangers. From that viewpoint, then, the best temperature difference across the thermoelectric modules would be only one-half of the total air–ground temperature difference. The second consideration is that the air-side heat exchanger benefitted from direct solar insolation and so regularly produced more power than would be indicated by the air–ground temperature difference. This will be considered in detail in the analysis.

Figs. 4a and 4b shows the temperatures at the center of the air-side heat exchanger, at the top surface of the insulator on the top of the upper thermoelectric module, the bottom surface on the insulator on the bottom of the lower thermoelectric module, and the center of the ground-side heat exchanger. Fig. 4a shows results for the unfinned prototype while Fig. 4b shows results for the finned prototype. Both 4a and 4b correspond to the first period shown in Fig. 3a. As expected, the temperature drop through the heat exchangers is relatively small for both cases. Neglecting the temperature drop through the ceramic insulators, which is also expected to be small, Figs. 4a and 4b primarily illustrates the temperature difference across the two thermoelectric modules. This will be the temperature difference relevant to power generation from the prototype devices.

Figs. 5a and 5b demonstrates all temperature differences, and illustrates where the temperature drops occur through the system. For reference, the total temperature difference between the air and the ground is shown on an area plot in the upper part of the figure with the right-side axis. All other temperature differences are shown on the left-side axis. The solid line and the dashed line show, respectively, the temperature differences between the air and the air-side heat exchanger, and between the ground-side heat

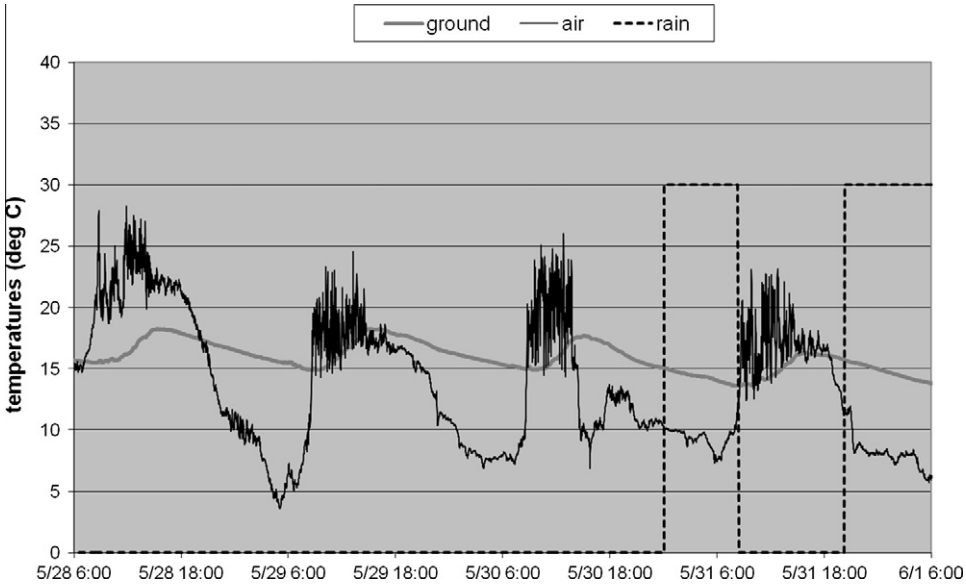


**Fig. 3a.** Air and ground temperatures, first period.

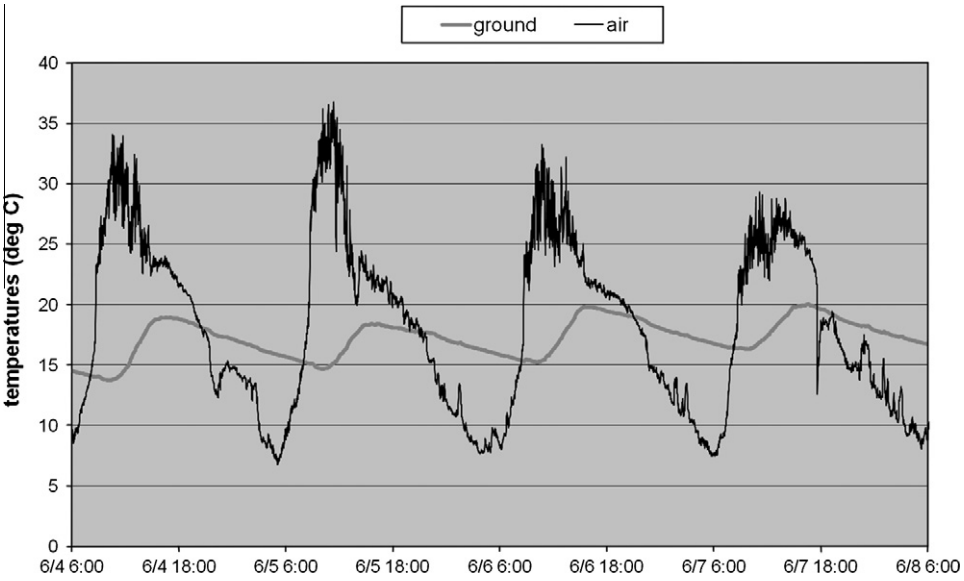


**Fig. 3b.** Air and ground temperatures, second period.

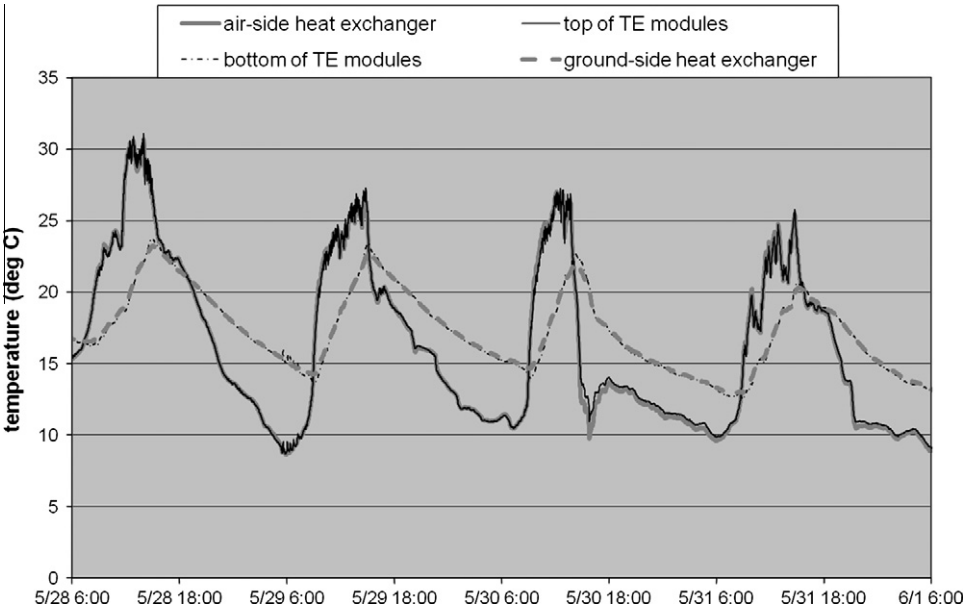


**Fig. 4a.** Prototype temperatures, unfinned.

exchanger and the ground. The other temperature differences are shown in a stacked area plot on the lower part of Figs. 5a and 5b. The largest area (cream-colored) corresponds to the temperature difference across the thermoelectric modules. The small black and grey areas which are barely visible in a few spots along the edges represent temperature drops through the heat exchangers. This graphically emphasizes that the largest temperature drops occur on the heat exchanger surfaces and through the thermoelectric modules. Fig. 5a is for the unfinned prototype, and Fig. 5b is for the finned version.

Comparison of the total air–ground temperature difference area plot in the top part of the figure with the white portion of the stacked area plot in the lower part gives a qualitative feel for the fraction of the total air–ground temperature drop that is available for power generation. Inspection shows that the temperature drops from the air to the air-side heat exchanger and from the ground-side heat exchanger to the ground constitute the most significant portions. This figure also illustrates the phase-shift in temperature differences resulting from the effects of the transient heat transfer processes. Compare, for example, the locations of the peaks in the dashed line representing the temperature difference between the ground-side heat exchanger and the ground with the locations of the peaks in the white area plot representing the temperature difference across the thermoelectric modules. Finally, effects of direct solar insolation are also clearly visible in this figure. Comparing the second positive peaks in Fig. 5b, for example, shows that the temperature drop across the thermoelectric modules is greater than the temperature difference between the air and the ground. This is due in part to the direct solar heating of the air-side heat exchanger.

Figs. 6a and 6b shows a direct comparison between the instantaneous power generation for the finned and unfinned prototypes

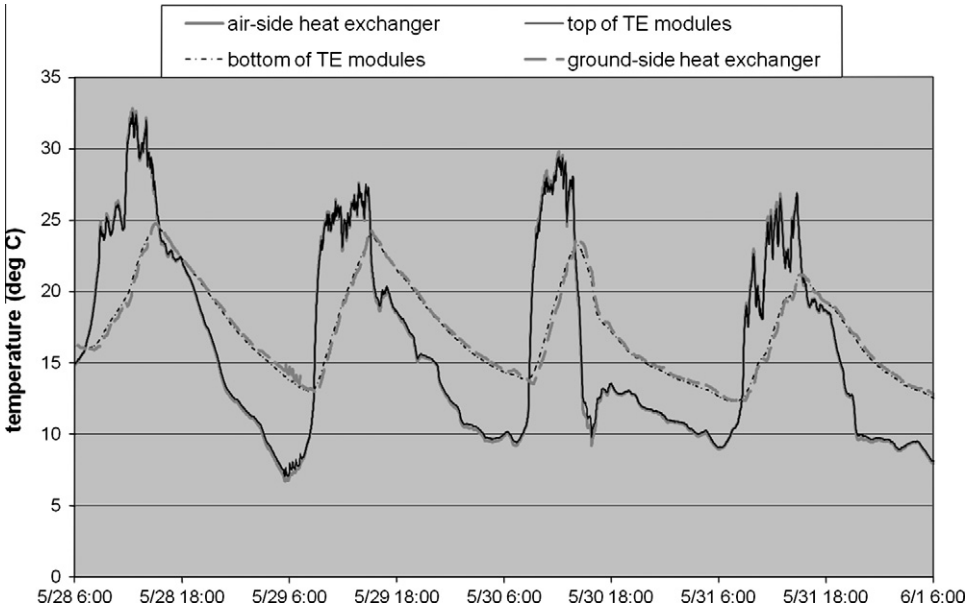


**Fig. 4b.** Prototype temperatures, finned.

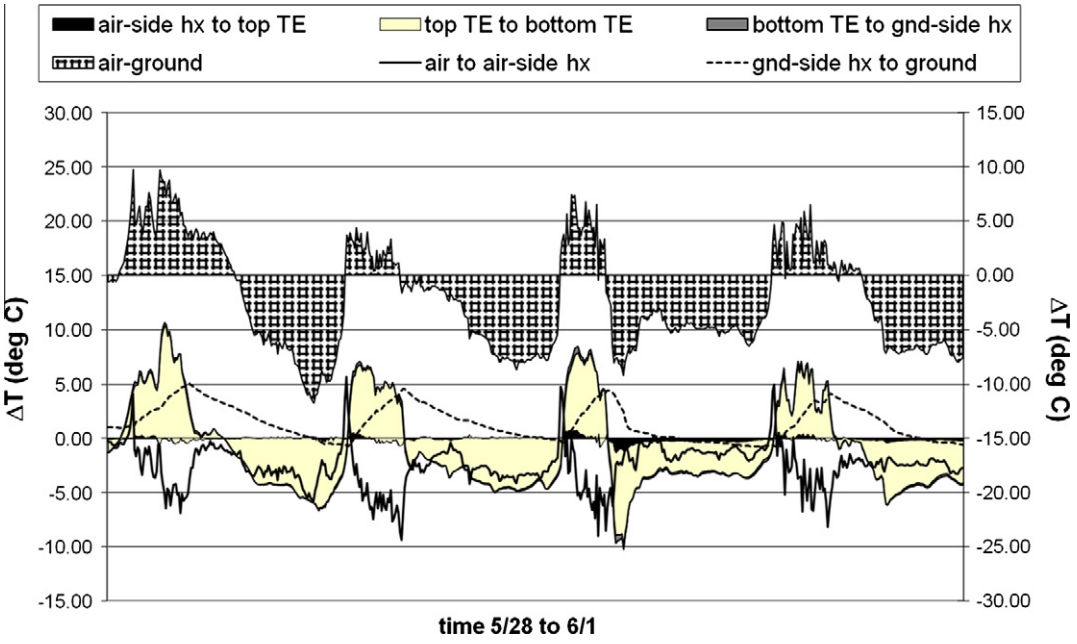


**Fig. 5a.** Temperature drops, unfinned configuration.

for the two four day periods presented in Figs. 3a and 3b. The twice daily excursions to zero power are clearly visible, as are the differences between daytime and nighttime generation performance. These results are very similar to the numerical predictions of Agbossou et al. [15] for a thermoelectric generator coupled to a phase change material. They also bear a remarkable similarity to the analytically predicted electrical output based on measured thermal conductances of Lawrence and Snyder [12]. Averaged over the full 25 day trial period, including daytime, nighttime, and overcast day performance, the unfinned prototype generated 685 μW while the finned prototype generated at an average rate of 1046 μW.

Figs. 7a and 7b presents the total electrical energy generated over the 25 day test period by hour-of-the-day for both prototypes. Fig. 7a shows the generation by total energy, and Fig. 7b by percentage for each prototype. The most striking feature of these figures is the large effect that direct sunlight has on the power generation capacity. While it may be noted from Figs. 3a and 3b that the air–ground temperature differences tend to be slightly larger during day, and the power generation is proportional to the square of the temperature difference, that still would not adequately account for the disproportionate amount of energy that is produced between 9 am and 3 pm. From Fig. 7b, 78.0% of the total energy for the finned case and 75.6% for the unfinned case is generated during those hours. As previously indicated, direct solar insolation on the air-side heat exchanger accounts for the differences. A very rough estimate of that effect can be made by comparing the generation from the hours of 9 am to 3 pm with that of the

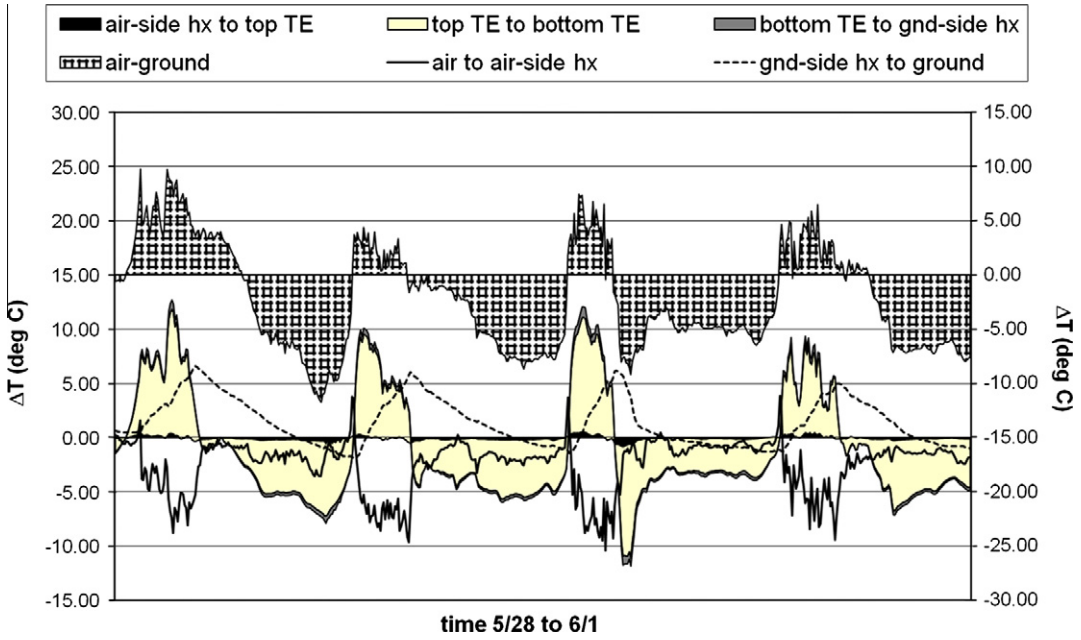


**Fig. 5b.** Temperature drops, finned configuration.

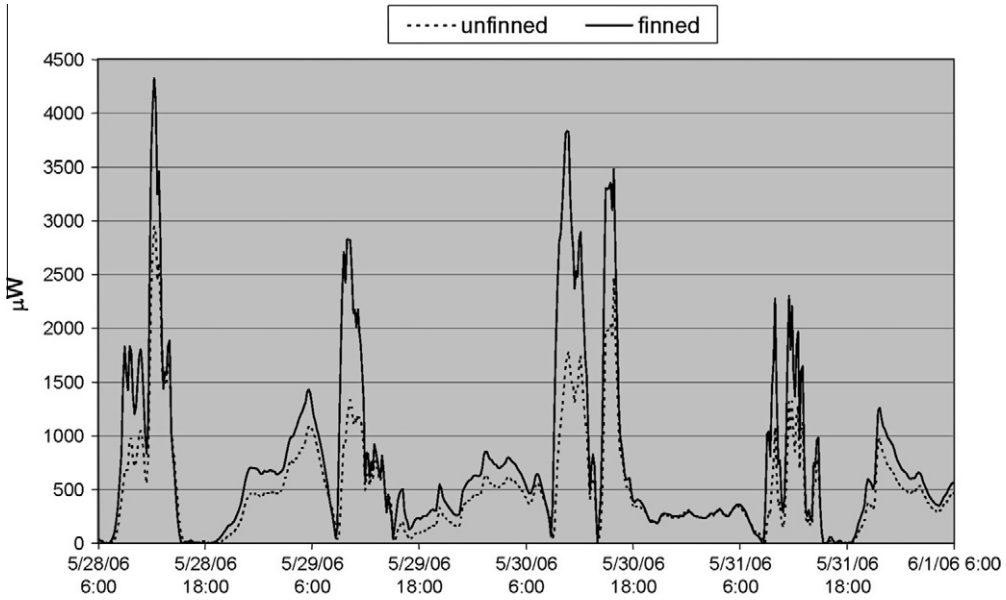


**Fig. 6a.** Instantaneous power generation, first period.

hours from 1 am to 7 am (which, from inspection of Fig. 7b contains the nighttime peak generation). Those numbers are 11.1% and 12.6% for the finned and unfinned cases, respectively. Thus, it might be conservatively estimated that over half of the total electrical energy generation can be attributed to heating by direct solar insolation on the air-side heat exchanger. Agbossou et al. [15] reported a similar disproportionate generation between daytime and nighttime in their numerical study of a thermoelectric generator coupled with a phase change material.

Figs. 8a and 8b shows the temperature drop across the thermoelectric modules plotted as a function of the total air–ground temperature difference. The different symbols represent three divisions of the day: midnight to 8 am, 8 am–4 pm, and 4 pm to midnight. Fig. 8a is for the unfinned prototype and Fig. 8b is for the finned prototype. In both plots, a line with slope equal to unity is included for reference. Two distinct regimes are evident in these plots. For the daytime hours, 8 am to 4 pm, the temperature differences fall predominantly into the upper right quadrant, extend to temperature differences close to 20 °C, and are spread on both sides of the unity slope line. For the two groups covering 4 pm–8 am, the points are closer to the origin, extending only to temperature differences of −10 °C. Of course, these differences merely provide a different qualitative perspective on features pointed out earlier: the effects of phase shift and direct solar insolation, and the resulting higher power generation during daylight hours. However, these plots can also be used to make a quantitative estimate for the overall factor by which the air–ground temperature difference must be scaled for estimating the thermoelectric

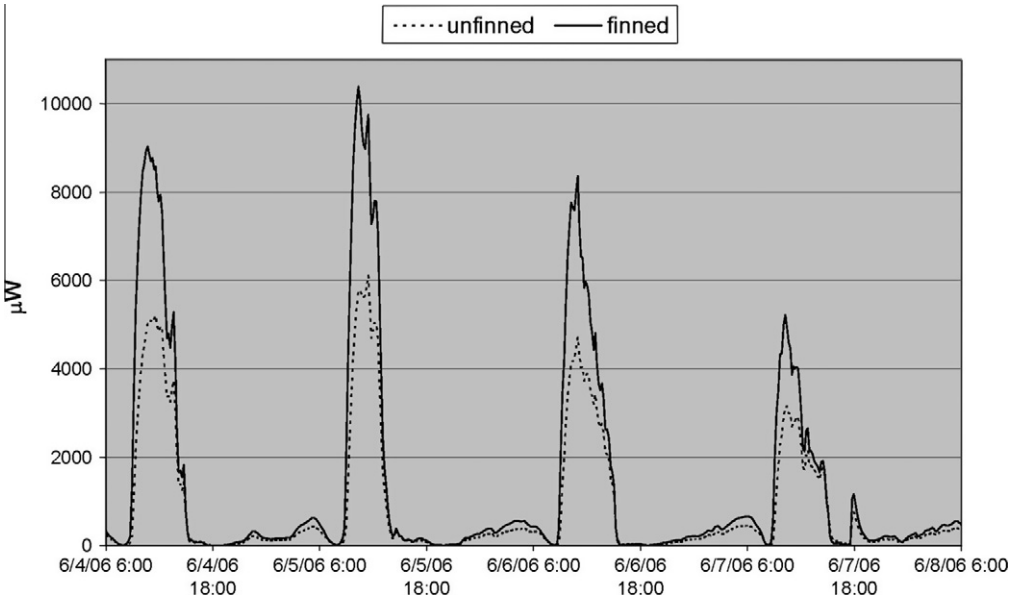


**Fig. 6b.** Instantaneous power generation, second period.

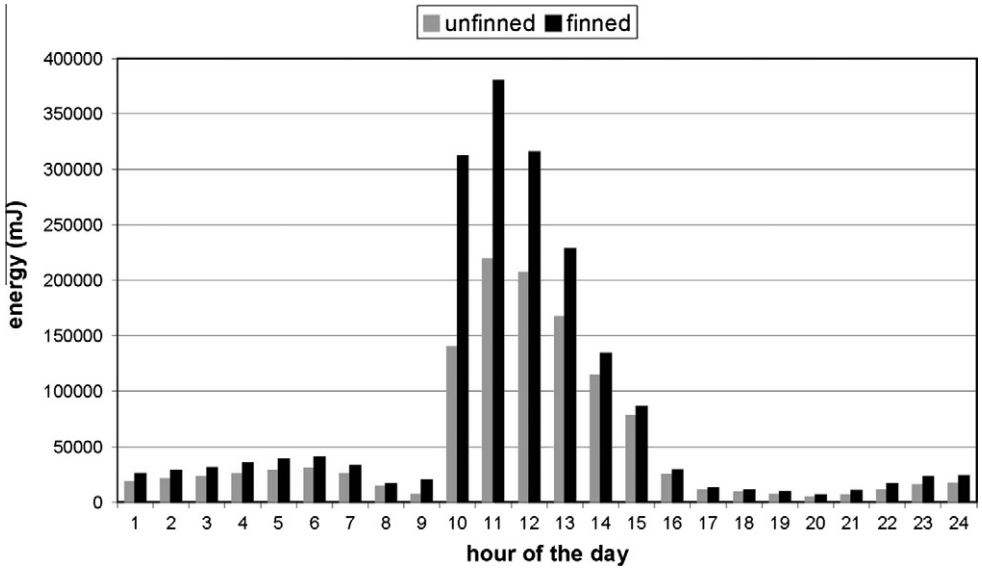


**Fig. 7a.** Total energy production binned by time-of-day.

module temperature drop. Table 1 shows the slope of regression lines for each of the data sets in Figs. 8a and 8b.

The effects of phase shift and direct solar heating bring the scaling factor close to unity for the daytime hours, while the appropriate factor for the remaining hours is in the neighborhood of one-half. An optimal design would divide the total temperature drop evenly between the heat exchangers and the thermoelectric modules. This design, which seemed to allocate too little $\Delta T$ to the thermoelectric modules according to thermal resistance estimates turned out to be fairly good without considering the effect of direct solar insolation.

Transient heat transfer effects and the imposition of direct solar heating complicate efforts to estimate and compare thermal resistances between components of the finned and unfinned prototypes. The thermal resistance concept is based on quasi steady-state heat transfer while the case under consideration is changing constantly with time. However, thermal resistance provides a very convenient characterization for the heat transfer processes involved. Furthermore, all transient changes occur slowly relative to the thermal inertia of the system components and all processes occur cyclically so it may be expected that the transient effects may cancel out by considering multiple cycles. By restricting consideration of data to those hours where there is no direct sunlight, a rough estimate of actual thermal resistances may be obtained as follows:

For the small $\Delta T$ involved in this application, the manufacturer's literature suggests that the efficiency of the thermoelectric module is a linear function of the temperature difference which can be expressed using a constant of proportionality, $\alpha$, as:

$$\eta = \alpha \Delta T$$

Since the thermal resistance is defined as:

$$R_{\text{th}} \equiv \Delta T / Q$$

and the efficiency is:

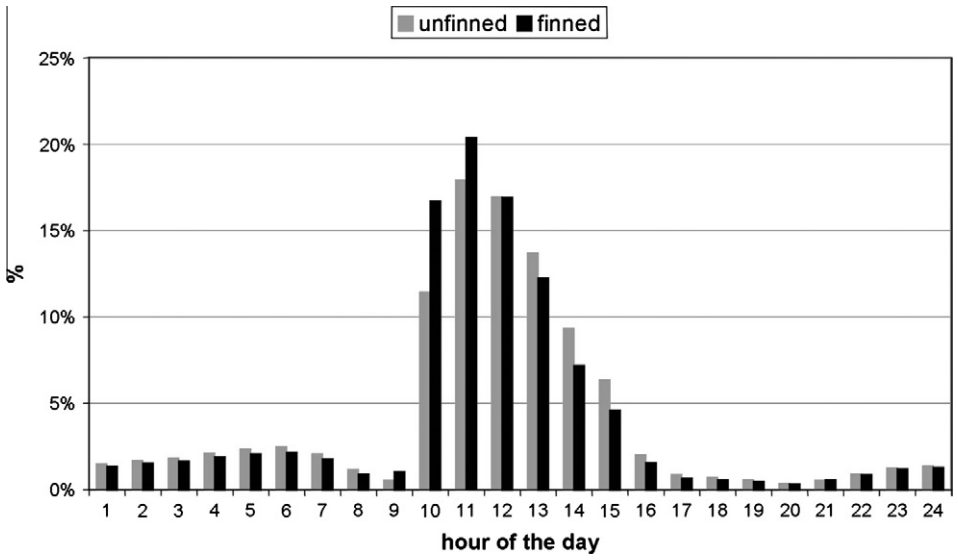


**Fig. 7b.** Percentage energy production binned by time-of-day.

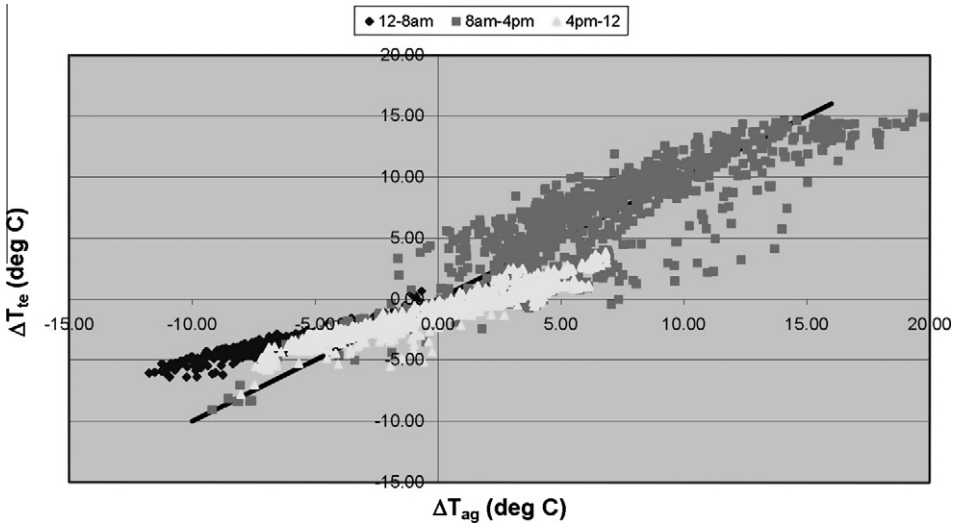


**Fig. 8a.** Temperature differences for the unfinned configuration.

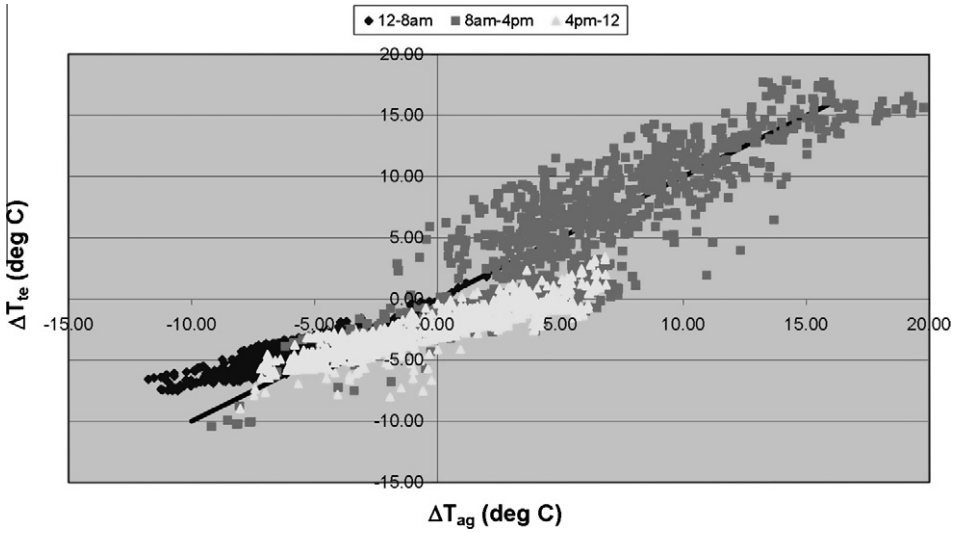


**Fig. 8b.** Temperature differences for the finned configuration.

**Table 1**
Scaling factors from slope.

| | Unfinned | Finned |
|---|---|---|
| 12–8 am | 0.44 ± 0.005 | 0.55 ± 0.010 |
| 8 am–4 pm | 0.84 ± 0.016 | 0.97 ± 0.019 |
| 4 pm–12 | 0.52 ± 0.006 | 0.50 ± 0.009 |

**Table 2**
Estimated thermal resistances (K/W).

| | Air to air-side hx | Air-side hx | TE modules | Gnd-side hx | Gnd-hx to ground |
|---|---|---|---|---|---|
| Unfinned | 17.2 ± 0.86 | 3.7 ± 0.23 | 10.5 ± 0.25 | 3.7 ± 0.22 | 19.7 ± 1.06 |
| Finned | 8.3 ± 0.31 | 3.1 ± 0.16 | 13.3 ± 0.39 | 2.7 ± 0.14 | 5.3 ± 0.28 |

$$\eta \equiv W/Q$$

The heat flow, $Q$, can be eliminated to provide an estimate for thermal resistance in terms of the measured output power, $W$:

$$R_{th} = \alpha \Delta T^2 / W$$

Using this relationship, the thermal resistance for various components is estimated as presented in Table 2 with a 95% confidence interval.

The fins appear to reduce the overall thermal resistance at the air and ground interfaces by a factor of two to four while having a small effect on the already small thermal resistance through the heat exchangers. The manufacturer's literature suggests that the thermal resistance through two modules in series should be around 5 K/W. The estimate presented in Table 2 includes the contact resistance between the thermoelectric modules and the ceramic insulator plates, as well as the thermal resistance through a total of three ceramic plates. In design calculations, the additional thermal resistance, (including thermal grease to reduce contact resistance) was estimated at 0.08 K/W. This suggests that the contact resistance is significantly higher than originally anticipated.

## 6. Conclusions and summary

An extended performance evaluation of a finned and an unfinned version of a prototype ground-source thermoelectric generator was conducted. It was confirmed that the predominant temperature drops occurred at the interfaces between the air-side heat exchanger and the air and between the ground-side heat exchanger and the ground. Using 2 HZ-2 thermoelectric modules in series (each $1.15'' \times 1.15'' \times 0.2''$) the unfinned prototype produced power at a long-term average rate of 685 μW and the finned prototype produced power at an average rate of 1046 μW. Direct solar insolation contributed significantly to the total power generation. A rough estimate indicates that this effect might be responsible for over half of the total electrical energy generation. With the effects of direct solar insolation and transient heat transfer, a working estimate of the total air–ground temperature difference that is available to the thermoelectric modules for power generation is in the range of 50–100%. A rough estimate of the thermal resistance of various components of the finned and unfinned prototypes indicated that the fins might reduce the air-side and ground-side predominant thermal resistances by a factor of 2–3. It also appeared that the contact resistance between surfaces might be significantly higher than typical estimates.

## References

[1] Stevens JW. Optimal placement depth for air–ground heat transfer systems. Appl Thermal Eng 2003;24:149–57.
[2] Lemley LW. A radiation thermoelectric power converter. In: Proceedings of the third international conference on thermoelectric energy conversion. Arlington, TX, USA: IEEE, NY, NY; 1980. p. 20–6.
[3] Wu C. Analysis of waste-heat thermoelectric power generators. Appl Thermal Eng 1996;16(1):63–9.
[4] Wu C. Performance of solar-pond thermoelectric power generators. Int J Ambient Energy 1995;16(2):59–66.
[5] Benson DK, Jayadev TS. Thermoelectric energy conversion, economical electric power from low grade heat. In: Proceedings of the Third International Conference on Thermoelectric Energy Conversion. Arlington, TX, USA: IEEE, NY, NY; 1980. p. 27–56.
[6] Chen J. Thermodynamic analysis of a solar-driven thermoelectric generator. J Appl Phys 1996;79(5):2717–21.
[7] Henderson J. Analysis of a heat exchanger-thermoelectric generator system. In: Proceedings of the 14th intersociety energy conversion engineering conference, vol. 2. Boston, MA, USA, August 5–10; 1979. p. 1835–40.
[8] Hudak NS, Amatucci GG. Small-Scale Energy Harvesting Through Thermoelectric, Vibration, and Radiofrequency Power Conversion. J Appl Phys 2008;103:101301.
[9] Thomas JP, Qidwai MA, Kellogg JC. Energy scavenging for small-scale unmanned systems. J Power Sour 2006;159:1494–509.
[10] Dalola S, Ferrari M, Ferrari V, Guizzetti M, Marioli D, Taroni A. Characterization of thermoelectric modules for powering autonomous sensors. IEEE Trans Instrum Meas 2009;58(1):99–107.
[11] Sodano HA, Simmers GE, Dereux R, Inman DJ. Recharging batteries using energy harvested from thermal gradients. J Intell Mater Syst Struct 2007;18:3–10.
[12] Lawrence EE, Snyder GJ. A study of heat sink performance in air and soil for use in a thermoelectric energy harvesting device. In: Proceedings of the twenty-first international conference on thermoelectrics ICT 02; 2002. p. 446–9.
[13] Meydbray Y, Singh R, Shakouri A. Thermoelectric module construction for low temperature gradient power generation, In: Proceedings of the twenty-fourth international conference on thermoelectrics ICT 05; 2005. p. 348–51.
[14] Snyder GJ. In: Priya, Inman, editors. Thermoelectric energy harvesting. Energy Harvesting Technologies: Springer; 2009. p. 325–36.
[15] Agbossou A, Zhang Q, Sebald G, Guyomar D. Solar micro-energy harvesting based on thermoelectric and latent heat effects. Part I: theoretical analysis. Sensors Actuat A: Phys 2010;163:277–83.
[16] Stevens JW. Optimal design of small $\Delta T$ thermoelectric generation systems. Energy Convers Manage 2001;42:709–20.